Spring 5-2-2011

Effects of Gas Velocity and Solid Hold-Up on the Sub-Grid Behavior of Riser Flows

Christian Costa Milioli
University of São Paulo, School of Engineering of São Carlos, Dept. of Mech. Engng, ccosta@sc.usp.br

Fernando Eduardo Milioli
University of São Paulo, School of Engineering of São Carlos, Dept. of Mech. Engng, milioli@sc.usp.br

EFFECTS OF GAS VELOCITY AND SOLID HOLD-UP ON THE SUB-GRID BEHAVIOR OF RISER FLOWS

Christian Costa Milioli [1] and Fernando Eduardo Milioli [2]

University of São Paulo, School of Engineering of São Carlos, Dept. of Mech. Engng.,
Av. Trabalhador São-carlense, 400, 13566-590, São Carlos, SP, Brazil.
[1] ccosta@sc.usp.br; [2] milioli@sc.usp.br

ABSTRACT

Two-fluid highly resolved sub-grid simulations (SGS) of riser flows were developed under realistic gas velocities and solid hold-ups, for a solid phase derived from high Stokes number particles. The results showed that both gas velocity and solid hold-up considerably affect the effective hydrodynamics of the solid phase.

INTRODUCTION

Large scale simulations (LSS) with two-fluid models are expected, in time, to provide accurate predictions of real scale riser flows. One related aspect requiring attention is the proposition of sub-grid closures for solid phases. Along this last decade some researchers have been trying to draw those closures from sub-grid scale simulations (SGS) with two-fluid models. Among the relevant works on that matter are those of Sundaresan (1), Agrawal et al. (2), Andrews IV et al. (3), van der Hoef et al. (4) and Igci et al. (5). Those works take advantage of the fact that, regarding solid phases, highly resolved simulations are feasible in computational domains that are large enough to fit LSS numerical cells. Under suitable grid refinements a single SGS step can directly provide closures for LSS of real riser flows. The micro-scale description of the solid phase that is required in SGS is brought from the kinetic theory of granular flows (KTGF) (6,7,8,9). The common SGS computational experiment is performed in small periodic domains which are thought to repeat themselves throughout the whole volume of a riser. As periodic boundaries are applied an additional gas phase pressure gradient is introduced in the gravitational direction to account for the flow driving force. Such additional term is chosen to exactly match the gravity acting on the average gas-solid mixture, so that the simulations give rise to low velocity gas-solid flows. In spite of that, the clustering mechanism that prevails is believed to be relevant to rapid gas-solid flows (10,11).

In a recent work by Benyahia (12), a filtered drag model derived from the sub-grid data of Igci et al. (5) was applied to the LSS of a riser flow. The author's comparison of predictions against experiment showed considerable discrepancies, indicating that SGS under periodic boundaries requires enhancement. The present article is an attempt to contribute to the discussion on that matter by performing SGS under riser realistic conditions of gas velocity and solid hold-up. It is proposed, differently from all the previous work, to apply an additional gas phase pressure gradient in excess of that required to match the gravity acting on the local gas-solid mixture. In this case

the flow becomes accelerated and instantaneous field predictions are found through a range of gas velocities. While those predictions at any particular mesh point should not be regarded as significant in view of the instability of the flow, the domain average results, on the other hand, are thought to be quite representative. Simulations were developed for a range of domain average solid volume fractions, and results were analyzed in a range of gas phase axial velocities typical of riser flows. The effect of those parameters were evaluated over the flow topology, the average slip velocity, the effective stresses of the solid phase, and the effective drag. A solid phase was considered which is derived from a high Stokes number particulate typical of circulating fluidized bed combustors and gasifiers.

MATHEMATICAL MODELLING

Multiphase flow two-fluid models stand on the major hypothesis of continuum for all of the phases, no matter fluid or particulate. The phases are treated as inter-penetrating dispersed continua in thermodynamic equilibrium. The theory of two-fluid models has been developed by many researchers. Some classical references on this matter are due to Gidaspow (9), Anderson and Jackson (13), Ishii (14), Drew (15), Enwald et al. (16), among many others. The hydrodynamic two-fluid models comprise a basic set of average mass and momentum conservative equations plus closure laws for stress tensors, viscosities, pressures and drag.

The present two-fluid model is formulated to perform SGS, which remains LSS alike regarding the gas phase, but is required to become highly resolved regarding the solid phase so that all the scales of clusters are captured. In this way, the gas phase would require closures at both the micro and the meso-scales. Literature shows that under high Stokes numbers, which is the present case, the turbulence of the fluid phase has little effect over the solid (2,17). As the concern in the present analysis is the behavior of the solid phase, no turbulence model is applied for the gas phase. The micro-scale closure for the solid phase is established by applying the kinetic theory of granular flows (KTGF), where solid phase micro-scale properties are derived as a function of a granular temperature determined from a pseudo thermal energy balance. In this work, for the sake of simplicity, the algebraic approach of Syamlal et al. (18) is applied, where the pseudo thermal energy is assumed to be locally generated by viscous stress and dissipated by inelastic collisions. Table 1 presents the sub-grid scale hydrodynamic formulation that was applied, where the gas phase continuity and momentum equations come from Favre averaging over the respective filtered equations. Periodic conditions are applied at entrance and exit, i.e. in the horizontal boundaries normal to the vertical gravitational direction. An additional gas phase pressure gradient is enforced in that direction to account for the flow driving force. Free slip is applied in all of the vertical boundaries. Agrawal et al. (2) showed that the application of either free slip, partial slip, or periodic conditions to vertical boundaries gives rise to the same flow topology. In the present work the simpler free slip condition was applied. Solid phase's effective stresses and effective drag are determined from the SGS predictions by applying the relations in Table 2. The effective stress tensor is derived by Favre averaging over the filtered solid phase momentum equation. As a filter size is applied that exactly fits the sub-grid domain, the filtered parameters become equal to their volume averages. Following literature (4,5) the filtered drag force was expressed as a function of an effective drag coefficient and the filtered slip velocity, thereby providing a relation for the effective drag coefficient.

Table 1. Sub-grid scale hydrodynamic formulation of the two-fluid model.

$$\frac{\partial}{\partial t}\left(\rho_g \bar{\alpha}_g\right) + \nabla\cdot\left(\rho_g \bar{\alpha}_g \tilde{\boldsymbol{u}}_g\right) = 0$$

$$\frac{\partial}{\partial t}\left(\rho_s \alpha_s\right) + \nabla\cdot\left(\rho_s \alpha_s \boldsymbol{u}_s\right) = 0$$

$$\frac{\partial}{\partial t}\left(\rho_g \bar{\alpha}_g \tilde{\boldsymbol{u}}_g\right) + \nabla\cdot\left(\rho_g \bar{\alpha}_g \tilde{\boldsymbol{u}}_g \tilde{\boldsymbol{u}}_g\right) = -\bar{\alpha}_g\left(\nabla \tilde{P}_g + \psi \nabla P_g^*\right) + \nabla\cdot\left[\bar{\alpha}_g\left(\tilde{\boldsymbol{\tau}}_g - \boldsymbol{\tau}_{ge}\right)\right] + \rho_g \bar{\alpha}_g \boldsymbol{g} + \tilde{\boldsymbol{M}}_{gI}$$

$$\frac{\partial}{\partial t}\left(\rho_s \alpha_s \boldsymbol{u}_s\right) + \nabla\cdot\left(\rho_s \alpha_s \boldsymbol{u}_s \boldsymbol{u}_s\right) = -\alpha_s\left(\nabla \tilde{P}_g + \psi \nabla P_g^* + \nabla P_s\right) + \nabla\cdot\left(\boldsymbol{\tau}_s\right) + \alpha_s \rho_s \boldsymbol{g} + \boldsymbol{M}_{sI}$$

$$\bar{\alpha}_g + \alpha_s = 1$$

$$\nabla P_g^* = \left(\rho_s \alpha_s + \rho_g \bar{\alpha}_g\right)\boldsymbol{g}$$

$$\tilde{\boldsymbol{\tau}}_g = \bar{\mu}_g\left[\nabla \tilde{\boldsymbol{u}}_g + \left(\nabla \tilde{\boldsymbol{u}}_g\right)^T\right] - \tfrac{2}{3}\bar{\mu}_g\left(\nabla\cdot\tilde{\boldsymbol{u}}_g\right)\boldsymbol{I}$$

$$\boldsymbol{\tau}_s = \mu_s\left[\nabla \boldsymbol{u}_s + \left(\nabla \boldsymbol{u}_s\right)^T\right] + \left(\lambda_s - \tfrac{2}{3}\mu_s\right)\left(\nabla\cdot\boldsymbol{u}_s\right)\boldsymbol{I}$$

$$\mu_s = \frac{4}{5}\alpha_s^2 \rho_s d_p g_0 (1+e)\left(\frac{\Theta}{\pi}\right)^{1/2} \qquad \lambda_s = \frac{4}{3}\alpha_s^2 \rho_s d_p g_0 (1+e)\left(\frac{\Theta}{\pi}\right)^{1/2} \qquad \text{(Gidaspow, 9)}$$

$$g_0 = \left[1 - \left(\frac{\alpha_s}{\alpha_{s,max}}\right)\right]^{-2.5\ \alpha_{s,max}} \qquad \text{(Lun and Savage, 19)}$$

$$P_s = \rho_s \alpha_s \Theta\left[1 + 2(1+e) g_0 \alpha_s\right] \qquad \text{(Gidaspow, 9)}$$

$$\Theta^{1/2} = \frac{-K_1 \alpha_s tr(\boldsymbol{D}_s) + \sqrt{K_1^2 tr^2(\boldsymbol{D}_s)\alpha_s^2 + 4K_4 \alpha_s\left[K_2 tr^2(\boldsymbol{D}_s) + 2K_3 tr\left(\boldsymbol{D}_s^2\right)\right]}}{2\alpha_s K_4} \qquad \text{(Syamlal et al., 18)}$$

$$\boldsymbol{D}_s = \frac{1}{2}\left[\nabla \boldsymbol{u}_s + \left(\nabla \boldsymbol{u}_s\right)^T\right] \qquad K_1 = 2(1+e)\rho_s g_0 \qquad K_2 = \frac{4 d_p \rho_s (1+e)\alpha_s g_0}{3\sqrt{\pi}} - \frac{2}{3}K_3$$

$$K_3 = \frac{d_p \rho_s}{2}\left\{\frac{\sqrt{\pi}}{3(3-e)}\left[1 + 0.4(1+e)(3e-1)\alpha_s g_0\right] + \frac{8\alpha_s g_0 (1+e)}{5\sqrt{\pi}}\right\} \qquad K_4 = \frac{12\left(1-e^2\right)\rho_s g_0}{d_p \sqrt{\pi}}$$

$$\boldsymbol{M}_{sI} = -\tilde{\boldsymbol{M}}_{gI} = -\bar{\beta}\left(\boldsymbol{u}_s - \tilde{\boldsymbol{u}}_g\right)$$

$$\bar{\beta} = 150\frac{\alpha_s^2 \bar{\mu}_g}{\bar{\alpha}_g\left(d_p \varphi_p\right)^2} + 1.75\frac{\rho_g \alpha_s \left|\tilde{\boldsymbol{u}}_g - \boldsymbol{u}_s\right|}{\left(d_p \varphi_p\right)} \qquad \text{for} \quad \alpha_s > 0.2 \quad \text{(Ergun, 20; Gidaspow, 9)}$$

$$\bar{\beta} = \frac{3}{4} C_{Ds}\frac{\rho_g \alpha_s \bar{\alpha}_g \left|\tilde{\boldsymbol{u}}_g - \boldsymbol{u}_s\right|}{\left(d_p \varphi_p\right)}\left(\bar{\alpha}_g\right)^{-2.65} \qquad \text{for} \quad \alpha_s \le 0.2 \quad \text{(Wen and Yu, 21; Gidaspow, 9)}$$

$$C_{Ds} = \begin{cases} \dfrac{24}{\bar{R}e_p}\left(1 + 0.15\,\bar{R}e_p^{\,0,687}\right) & \text{for} \quad \bar{R}e_p < 1000 \\ 0.44 & \text{for} \quad \bar{R}e_p \ge 1000 \end{cases} \qquad \bar{R}e_p = \frac{\left|\tilde{\boldsymbol{u}}_g - \boldsymbol{u}_s\right| d_p \rho_g \bar{\alpha}_g}{\bar{\mu}_g} \qquad \text{(Rowe, 22)}$$

SIMULATIONS

The simulations were performed for a solid phase derived form a high Stokes number monodisperse particulate typical of low density risers (520 μm diameter, 2620 kg/m^3 density), and for solid phase average volume fractions of 0.015, 0.03, 0.05, 0.07 and 0.09. Accelerating flows were generated and the results were analysed for increasing gas velocities from about 3 to about 9 m/s. A 2x2 cm wide and 8 cm tall vertical hexahedral domain was considered, applying a 1x1x1 mm uniform hexahedral numerical mesh. The flow entered the domain through the bottom and exited at the top. The density and viscosity of the gas phase were, respectively, 1.1614 kg/m^3 and 1.82 x 10^{-5} N.s/m^2. A solid phase volume fraction at maximum packing of 0.38 was applied following Gidaspow and Ettehadieh (23), and a restitution coefficient of 0.9 was taken following Agrawal et al. (2).

Table 2. Solid phase's effective stresses and effective drag.

$$\boldsymbol{\tau}_{se} = \rho_s \overline{\alpha}_s \left(\widetilde{\boldsymbol{u}_s \boldsymbol{u}_s} - \widetilde{\boldsymbol{u}}_s \widetilde{\boldsymbol{u}}_s \right) = \rho_s \overline{\alpha}_s \left(\frac{\overline{\alpha_s \boldsymbol{u}_s \boldsymbol{u}_s}}{\overline{\alpha}_s} - \frac{\overline{\alpha_s \boldsymbol{u}_s}}{\overline{\alpha}_s} \cdot \frac{\overline{\alpha_s \boldsymbol{u}_s}}{\overline{\alpha}_s} \right) = \rho_s \left(\langle \alpha_s \boldsymbol{u}_s \boldsymbol{u}_s \rangle - \frac{\langle \alpha_s \boldsymbol{u}_s \rangle \cdot \langle \alpha_s \boldsymbol{u}_s \rangle}{\langle \alpha_s \rangle} \right)$$

$$\overline{\boldsymbol{M}}_{sI} = \overline{-\overline{\beta}(\boldsymbol{u}_s - \widetilde{\boldsymbol{u}}_g)} = -\left\langle \overline{\beta}(\boldsymbol{u}_s - \widetilde{\boldsymbol{u}}_g) \right\rangle \qquad \overline{\boldsymbol{M}}_{sI} = -\beta_e \left\langle \boldsymbol{u}_s - \widetilde{\boldsymbol{u}}_g \right\rangle \qquad \beta_e = \frac{\left\langle \overline{\beta}\left(\boldsymbol{u}_s - \widetilde{\boldsymbol{u}}_g\right) \right\rangle}{\left\langle \boldsymbol{u}_s - \widetilde{\boldsymbol{u}}_g \right\rangle}$$

The driving force factor (ψ) was set to 1.5. This value allowed the simulations to go along a suitable range of gas axial velocities in a reasonable computing time. Initial conditions for the accelerating runs were obtained by running previous simulations applying $\psi = 1$, departing from uniform quiescent suspensions with fixed uniform solid volume fractions. A time step of 5x10^{-5} s was applied which is suitable for solid phase highly resolved simulations. The lower characteristic time scale of clusters of the order of 10^{-2} s (24). Also, for the present 520 μm particulate size the smaller clusters on the flow are expected not to be larger than 5.2 mm (following 2). Therefore, regarding the solid phase, both the spatial and temporal meshes which were applied are suitable for highly resolved simulations. The convergence criterion for the numerical procedure was a rms of 1x10^{-5}. The simulations were carried out using the software Cfx (25).

RESULTS

The effects of the domain average solid volume fraction and gas phase axial velocity over the flow effective hydrodynamics were evaluated. The greyscale plots of solid phase fraction in Figure 1 show that the topology of the flow considerably changes by changing the concerning parameters. By increasing the average solid fraction, for a particular gas velocity, larger clusters are formed. By increasing the gas velocity, for a particular average solid fraction, the clusters become stretched in the axial direction.

Figure 2 shows plots of the effective stresses of the solid phase. Even though the results are very scattered, it is possible to observe that higher solid fractions give rise to higher stresses. The effective shear stresses seem not to change with gas velocity, while the normal stresses show considerable variations (e.g. drawn line in Fig. 2 (b)).

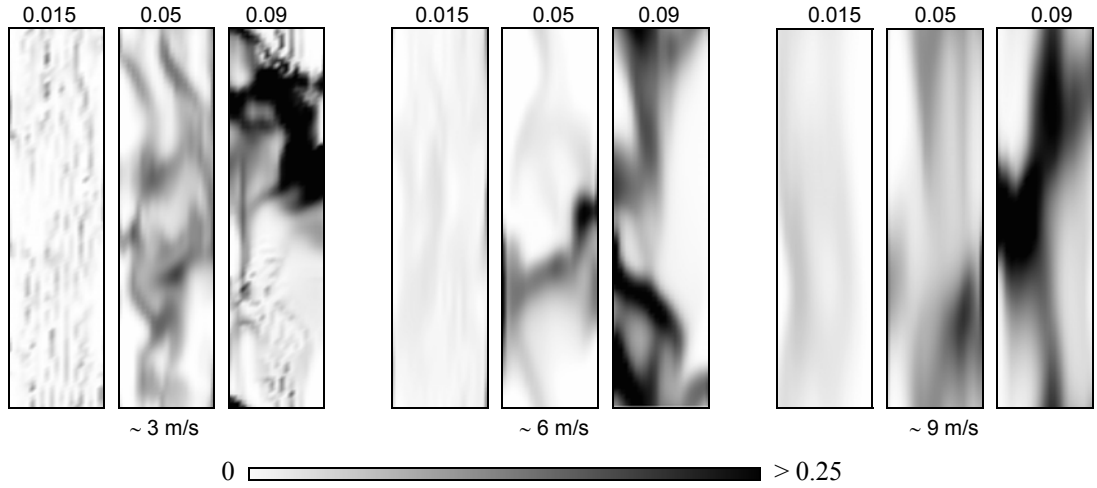

Figure 1. Solid volume fraction in an axial section of the domain for $\langle \alpha_s \rangle =$ 0.015, 0.05, 0.09, and $\langle \bar{v}_g \rangle \cong$ 3, 6, 9 m/s.

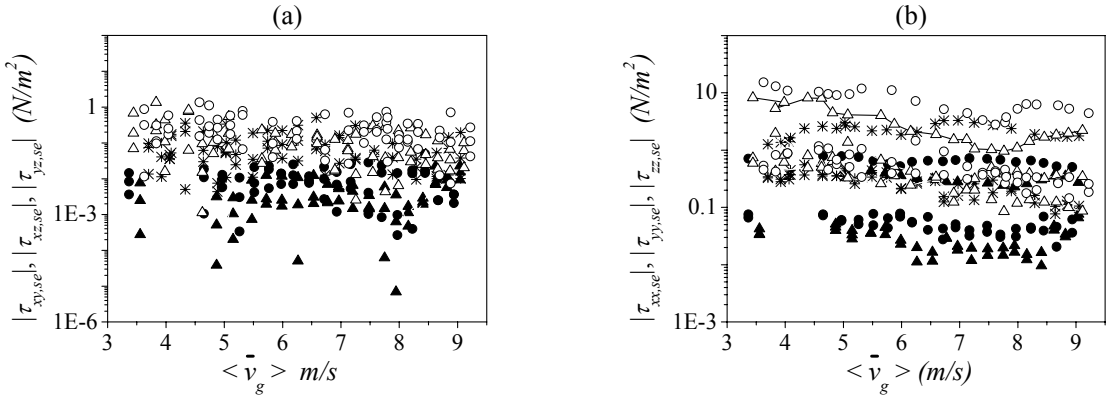

Figure 2. Effective shear (a) and normal (b) stresses of the solid phase as a function of $\langle \bar{v}_g \rangle$, for $\langle \alpha_s \rangle = 0.015$ (▲); 0.03 (●); 0.05 (∗); 0.07 (△) and 0.09 (○).

Figure 3 shows the behavior of the slip velocity and the effective drag coefficient. As seen, the higher the solid fraction, the lower the slip velocity, and the higher the effective drag coefficient. Both the parameters resulted little affected by the gas velocity, except for the slip velocity at higher solid fractions, where an oscillating behavior is also observed. This is possibly due to the formation of larger clusters in comparison to the size of the domain (see Fig. 1). Those oscillations are expected to disappear at sufficiently enlarged domains, that would always hold a considerable number of clusters throughout the whole range of gas velocities in an accelerating run. This issue, of course, requires verification.

Figure 4 brings some of the predictions compared to empirical data of Luo (26). This author performed experiments in a riser column with the same conditions applied in the current simulations. From the measurements, Luo determined effective shear stresses and effective drag coefficients for various average solid fractions. A few of those solid fractions, for a gas velocity close to 5 m/s, fall in the ranges considered in

the present simulations. As seen in Figure 4, Luo's results for those cases compare reasonably well with the present predictions, which is fine considering that Luo's results apply to regions close to the column wall, while the predictions are volume averaged over a free slip walls domain.

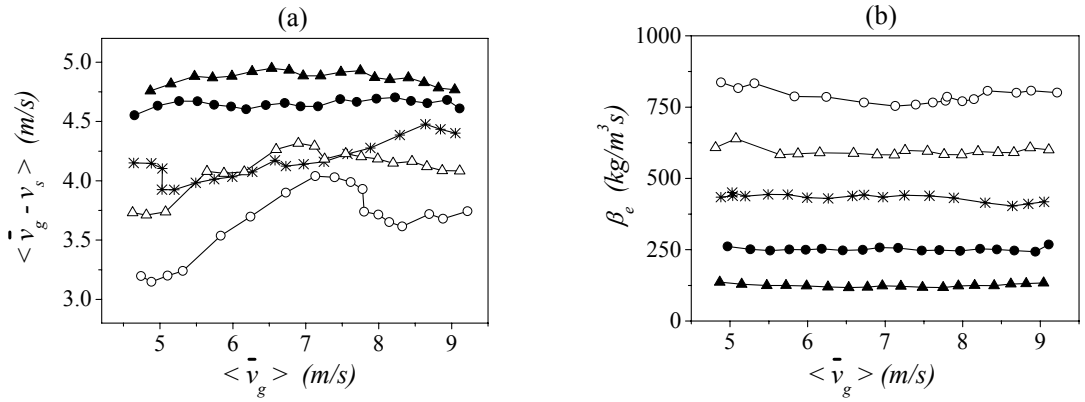

Figure 3. Slip velocity (a) and effective drag coefficient (b) as a function of $\langle \bar{v}_g \rangle$, for $\langle \alpha_s \rangle =$ 0.015 (▲); 0.03 (●); 0.05 (∗); 0.07 (△) and 0.09 (○).

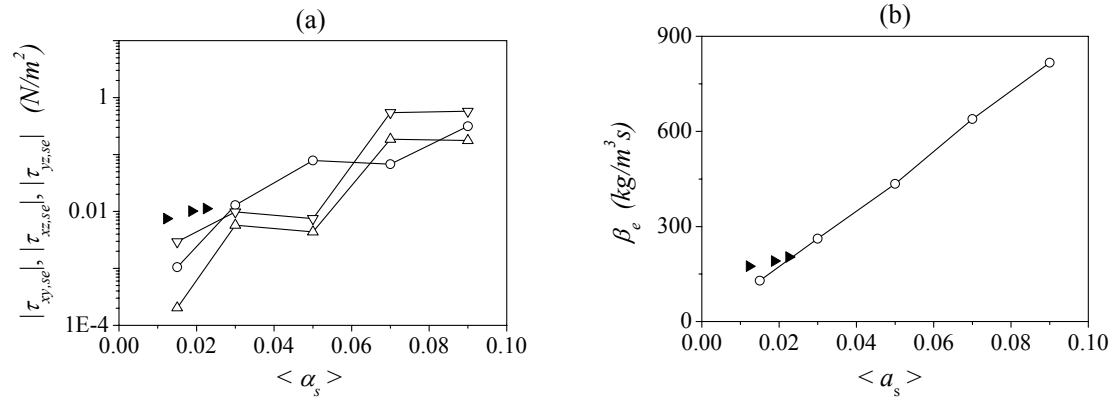

Figure 4. Effective shear stresses of the solid phase (a) and the effective drag coefficient (b) as a function of $\langle \alpha_s \rangle$, for $\langle \bar{v}_g \rangle \cong$ 5 m/s; (▸) empirical, Luo (26).

CONCLUSION

Two-fluid SGS was developed to investigate the sub-grid behavior of riser flows for a solid phase derived from a high Stokes number monodisperse particulate. Accelerated flow simulations were performed for a range of average solid fractions and gas velocities typical of risers. The effects of those parameters over the flow topology, the effective hydrodynamics of the solid phase and the effective drag were analyzed. The effects of both the gas velocity and the solid hold-up were found to be significant. A comparison was made of predictions against a few empirical data, and a reasonable agreement was found.

ACKNOWLEDGEMENTS

This work was supported by The State of São Paulo Research Foundation (FAPESP), The National Council for Scientific and Technological Development (CNPq), and The Coordination for the Improvement of Higher Level Personnel (CAPES).

NOTATION

C_D	drag coefficient (nd)	P	pressure (Nm^{-2})
d_p	particle diameter (m)	∇P^*	additional pressure gradient (Nm^{-3})
$\boldsymbol{D}$	strain rate tensor (s^{-1})	Re_p	particle Reynolds number (nd)
e	restitution coefficient (nd)	t	time (s)
$\boldsymbol{g}$	gravity acceleration (ms^{-2})	$\boldsymbol{u}$	velocity vector (ms^{-1})
g_0	radial distribution function (nd)	u, v, w	Cartesian velocities (ms^{-1})
$\boldsymbol{I}$	unit tensor (nd)	$\forall$	SGS domain volume (m^3)
$\boldsymbol{M}$	interface drag force (Nm^{-3})	x, y, z	Cartesian coordinates (m)

Greek letters

α	volume fraction (nd)	ρ	density (kgm^{-3})
β	friction coefficient ($kgm^{-3}s^{-1}$)	$\boldsymbol{\tau}$	viscous stress tensor (Nm^{-2})
Θ	granular temperature (m^2s^{-2})	$\boldsymbol{\tau}_e$	effective stress tensor (Nm^{-2})
λ	bulk viscosity (Nsm^{-2})	φ_p	particle sphericity (nd)
μ	dynamic viscosity (Nsm^{-2})	ψ	driving force factor (nd)

Subscripts

e	meso-scale or effective	max	maximum
g	gas phase	s	solid phase
I	interface	x, y, z	Cartesian directions

Others

$\overline{}$	LSS filtered (resolved)	$\sim$	Favre average, $\tilde{f} = \dfrac{\overline{\alpha f}}{\overline{\alpha}}$
$\langle ... \rangle$	volume average, $\langle f \rangle = \dfrac{1}{\forall}\int_{\forall} f \, d\forall$		

REFERENCES

1. Sundaresan, S. Modeling the hydrodynamics of multiphase flow reactors: current status and challenges. AIChE J. Vol. 46-6, pp. 1102-1105 (2000).
2. Agrawal, K., Loezos, P. N., Syamlal, M. and Sundaresan, S. The role of meso-scale structures in rapid gas-solid flows. J. Fluid Mech. Vol. 445, pp. 151-185 (2001).
3. Andrews IV, A. T., Loezos, P. N. and Sundaresan, S. Coarse-grid simulation of gas-particle flows in vertical risers. Ind. Eng. Chem. Res. Vol. 44-16, pp. 6022-6037 (2005).
4. van der Hoef, M. A., Ye, M., van Sint Annaland, M., Andrews IV, A. T., Sundaresan, S. and Kuipers, J. A. M., Multiscale modeling of gas-fluidized beds, Adv. Chem. Eng. Vol. 31, pp. 65-149 (2006).
5. Igci, Y., Andrews IV, A. T., Sundaresan, S., Pannala, S. and O'Brien, T. Filtered two-fluid models for fluidized gas-particle suspensions. AIChE J. Vol. 54-6, pp.

1431-1448 (2008).
6. Bagnold, R. A. Experiments on a gravity-free dispersion of large solid spheres in a Newtonian fluid under shear. Proc. R. Soc. Vol. A225, pp. 49-63 (1954).
7. Jenkins, J. T. and Savage, S. B. A Theory for the rapid flow of identical, smooth, nearly elastic spherical particles. J. Fluid Mech. Vol. 130, pp. 187-202 (1983).
8. Lun, C. K. K., Savage, S. B., Jeffrey, D. J. and Chepurniy, N. Kinetic theories for granular flows: inelastic particles in Couette flow and singly inelastic particles in a general flow field. J. Fluid Mech. Vol. 140, pp. 223-256 (1984).
9. Gidaspow, D. Multiphase flow and fluidization. San Diego. Academic Press (1994).
10. Goldhirsch, I., Tan, M. -L. and Zanetti, G. A molecular dynamical study of granular fluids I: the unforced granular gas in two dimensions. J. Sci. Comput. Vol. 8-1, pp. 1-40 (1993).
11. Tan, M. -L. and Goldhirsch, I. Intercluster interactions in rapid granular shear flows. Phys. Fluids Vol. 9-4, pp. 856-869 (1997).
12. Benyahia, S., On the effect of subgrid drag closures, Ind. Eng. Chem. Res., Vol. 49, pp. 5122-5131 (2010).
13. Anderson, T. B. and Jackson, R. Fluid mechanical description of fluidized beds. Equations of motion. Ind. Eng. Chem. Fund. Vol. 6, pp. 527-539 (1967).
14. Ishii, M. Thermo-fluid dynamic theory of two-phase flow. Paris. Eyrolles (1975).
15. Drew, D. A. Averaged field equations for two-phase media. Stud. Appl. Math. Vol. 1-2, pp.133-136 (1971).
16. Enwald, H., Peirano, E. and Almstedt, A. -E. Eulerian two-phase flow theory applied to fluidization. Int. J. Multiphase Flow. Vol. 22, pp. 21-66 (1996).
17. Fede, P. and Simonin, O. Numerical study of the subgrid fluid turbulence effects on the statistics of heavy colliding particles. Phys. Fluids Vol. 48, pp. 045103 (2006).
18. Syamlal, M, Rogers, W. and O´Brien, T. MFIX documentation theory guide. West Virginia. U.S. Department of Energy (1993).
19. Lun, C. K. K. and Savage, S. B. The effects of the impact velocity dependent coefficient of restitution on stresses developed by sheared granular materials. Acta Mech. Vol. 63, pp. 15-44 (1986).
20. Ergun, S. Fluid flow through packed columns. Chem. Eng. Prog. Vol. 48-2, pp. 89-94 (1952).
21. Wen, C. Y. and Yu, Y. U. Mechanics of fluidization. Chem. Eng. Prog. S. Ser. Vol. 62, pp. 100-111 (1966).
22. Rowe, P. N. Drag forces in a hydraulic model of a fluidized bed. Part II. Trans. Inst. Chem Eng. Vol. 39, pp. 175-180 (1961).
23. Gidaspow, D. and Ettehadieh, B. Fluidization in two-dimensional beds with a jet. Part II. Hydrodynamic modeling. Ind. Eng. Chem. Fund. Vol. 22, pp. 193-201 (1983).
24. Sharma, A. K., Tuzla, K., Matsen, J. and Chen, J. C. Parametric effects of particle size and gas velocity on cluster characteristics in fast fluidized beds. Powder Technol. Vol. 111, pp. 114-122 (2000).
25. Cfx, Discretization and solution theory. In Solver theory manual. Release 10. Waterloo. Ansys Canada (2005).
26. Luo, K. M., Experimental gas-solid vertical transport, PhD Thesis, Illinois Institute of Technology, Chicago, Illinois, (1987).